ACS OMEGA

http://pubs.acs.org/journal/acsodf

Article

Effects of Non-covalent Functionalization and Initial Mixing Methods on SWNT/PP and SWNT/EVOH Composites

Mahesh Parit and Virginia A. Davis*

Cite This: *ACS Omega* 2021, 6, 10618−10628

Read Online

ACCESS | Metrics & More | Article Recommendations | Supporting Information

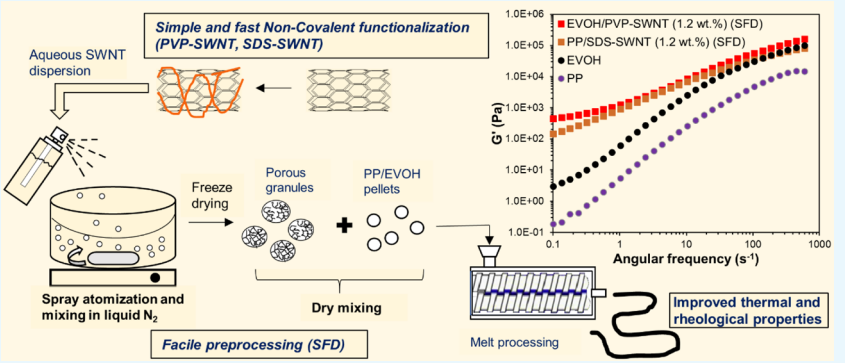

ABSTRACT: We report that a simple, low-cost type of spray-freeze drying (SFD) significantly improves the dispersion of single-walled carbon nanotubes (SWNTs) in thermoplastic polymers. Conventional SFD requires costly specialized equipment and large amounts of material, both of which are impediments to laboratory research on nanomaterial composites. Our method uses more readily available equipment and can be adapted to use milligrams to grams of material. A household spray bottle containing an aqueous nanomaterial dispersion is used to spray the dispersion into a dish of liquid nitrogen. The resulting material is then lyophilized in a standard laboratory freeze dryer. The usefulness of this simplified method was explored by comparing the properties of polypropylene (PP) composites produced by this method to those produced by a previously reported rotary evaporation method in which the dispersion is vacuum-dried onto the polymer. The role of the initial dispersion state was explored by using pristine SWNTs as well as SWNTs stabilized by two common SWNT stabilizers: polyvinylpyrrolidone (PVP) and sodium dodecyl sulfate. Based on rheological, thermal, and morphological characterization, the porous friable structures produced by SFD resulted in better SWNT dispersion compared to composites produced by a previously reported rotary evaporation method. However, the PP/PVP-SWNT nanocomposites produced by both methods contained large aggregates. To verify that this aggregation behavior was the result of thermodynamic incompatibility between PP and PVP, ethylene vinyl alcohol (EVOH) nanocomposites containing PVP-SWNT were also produced using the SFD method. The results of this research show how a low-cost alternative to SFD along with careful consideration of compatibility is a promising approach to produce nanocomposites.

1. INTRODUCTION

It is well established that single-walled carbon nanotubes (SWNTs) are one of the most challenging materials to disperse either in liquids or in polymer composites. The van der Waals attractions between SWNTs are 20−40 k_BT; for typical 500 nm long SWNTs, the attraction is more than an order of magnitude greater than that of a covalent bond.[1] As a result, avoiding aggregation in SWNT nanocomposites is a known challenge. However, there has been considerable interest in producing SWNT−polymer nanocomposites where the SWNTs' outstanding properties can be used to augment those of commodity polymers.[2−8] SWNTs can enable enhanced thermal stability and electromagnetic interference shielding. They can also improve heat transfer out of a material; SWNTs' thermal conductivity is over 3000 W/K·m, higher than the 2000 W/K·m value for diamond and the basal plane of graphite.[4,9] In addition, SWNTs' Young's modulus and tensile strength, calculated based on the normalized applied force per nanotube, are ∼0.64 TPa and ∼37 GPa, respectively. These values are close to Young's modulus of ∼0.66 TPa obtained for silicon carbide nanofiber and tensile strength of ∼53 GPa for silicon carbide nanorods. In fact, the density-normalized modulus and strength of SWNTs, which are important for applications requiring strong and light structural materials are ∼2.4 and

Received: December 18, 2020
Accepted: April 1, 2021
Published: April 14, 2021

~1.7 times that of silicon carbide nanorods and ~19 and ~56 times that of steel wire, respectively.[3,6−8] However, since the addition of SWNT aggregates will not result in property improvement, it is important to develop methods for achieving uniform dispersion of either individual SWNTs or small SWNT bundles that can form a percolated network and have significant interfacial interaction with the matrix.[10−12]

One approach to produce uniform nanocomposites is to dissolve the polymer in a solvent, add a dilute dispersion of nanomaterial in a liquid, and then remove the solvent after mixing. For example, Haggenmueller et al.[13] reported excellent SWNT dispersion and nanocomposite properties using a hot coagulation method where relatively dilute dispersions of SWNTs and polypropylene (PP) in hot dichlorobenzene were mixed and dried.[13] However, methods relying on the dissolution of the polymer in a solvent have disadvantages in terms of the time and cost of solvent removal, the negative environmental and health impacts of solvents such as dichlorobenzene, and the potential for polymer degradation.[14] Since composites produced using these methods will typically be melt-extruded into their final form, the majority of the literature has focused on producing melt-extruded composites. Much of the research has focused on simply dry mixing either pristine or covalently functionalized carbon nanotubes with polymers prior to melt extrusion.[15−19] However, pre-processing to increase the initial interfacial contact between the polymer and nanotubes can provide better results than dry mixing.[11,14] Zhang et al. employed the method of spraying the aqueous dispersion of sodium dodecylsulfate (SDS)-functionalized SWNTs directly onto a polymer followed by vacuum drying. The more uniform distribution of nanotubes prior to melt processing resulted in an improved dispersion state which led to a reduction in the rheological and electrical percolation thresholds.[20] Radhakrishnan et al. used a similar spray method where pristine SWNTs in isopropyl alcohol were sprayed onto polymer pellets or flakes and the solvent was removed by rotary evaporation (RE).[14] This RE method resulted in finer SWNT dispersion in PP, as indicated by thermal and rheological properties, than dry mixing. It resulted in less uniform dispersion than the hot coagulation method, but the hot coagulation method degraded the polymer.[13] Radhakrishnan et al. also explored the use of covalent SWNT functionalization with dodecyl groups in an effort to increase compatibility with the PP matrix but found that the functionalized SWNTs were not as well-dispersed as pristine SWNTs.

Compared to covalent functionalization, noncovalent functionalization has the advantage of attaching thermodynamically compatible groups or short polymer chains to nanotubes without decreasing their intrinsic properties by damaging their sp^2 hybridized structure.[21,22] Therefore, a number of researchers have shifted to looking at noncovalent SWNT functionalization for compatibilization with polymer matrices. Noncovalent functionalization also tends to be simpler and only requires a single-step, single-pot procedure where the SWNTs and dispersing agent are sonicated in water. It should be noted that although sonication debundles SWNTs and facilitates the interaction of the dispersant with SWNT sidewalls, it can also shorten the nanotubes' length.[10] SWNTs have been noncovalently functionalized with surfactants such as SDS, sodium octylbenzene sulfonate, sodium dodecylbenzene sulfonate, and dodecyl tri-methyl ammonium bromide[23,24] and copolymers such as poly(vinyl pyrrolidone) (PVP), poly(*m*-phenylene vinylene), poly(phenylene ethynylene), pluronic, and styrene-maleic anhydride.[24−28]

This research was inspired by Khoshkava and Kamal's finding that the use of a spray freeze dryer significantly improved dispersion in cellulose nanocrystal/polylactic acid composites[11] and a desire to see if spray-freeze drying (SFD) could similarly improve SWNT dispersion in polymers. SFD avoids the aggregation induced by capillary forces resulting from crossing the liquid−solid phase boundary, but commercial SFD equipment is both expensive and requires processing larger quantities of material than needed for small-scale production of nanocomposites. Therefore, Khoshkava and Kamal's method was modified to use more readily available equipment: a liquid nitrogen container, a consumer spray bottle, and a standard freeze dryer. This low-cost SFD method was compared to the RE method developed by Radhakrishnan et al.[14] using SWNTs and two common thermoplastics with different hydrophilicities: PP and ethyl vinyl alcohol (EVOH). In both cases, the pristine SWNTs were initially mixed with water. Since pristine SWNTs aggregate in water, it was thought that noncovalent functionalization could be used to improve the initial dispersion state and this would translate into the final polymer composite. SDS and PVP were chosen since they are two of the most commonly used materials for producing aqueous SWNT dispersions. SDS is the most widely used surfactant which interacts with SWNTs through non-specific hydrophobic interactions.[23,29] PVP is one of the best-known polymers for improving SWNT dispersion in water; it interacts with SWNTs via both the hydrophobic effect and CH−π interactions.[25]

The results of this research showed that for 0.75 wt % PP/SWNT and PP/EVOH, the simplified SFD method resulted in more uniform dispersion than the previously reported RE method.[14] However, it also highlighted that while the noncovalently functionalized SWNTs were better dispersed in the initial aqueous mixture, this did not necessarily result in a more uniform composite. In the case of PP/PVP-SWNTs, thermodynamic incompatibility between PP and PVP resulted in large aggregates in nanocomposites produced by both mixing methods. While this research has focused on SWNTs in two polymer matrices, the methods and findings can be applied to the development of processing schemes for other types of nanocomposites.

2. RESULTS AND DISCUSSION

2.1. Dispersion. Based on thermogravimetric analysis (TGA) in an inert atmosphere, the noncovalent functionalization resulted in PVP-SWNT and SDS-SWNT adducts which contained 47 and 40 wt % of the dispersion aide, respectively (Figure S1). The relatively large stabilizer to SWNT ratio is typical for noncovalent functionalization with these materials, and one of the potential disadvantages of the method. For this reason, the total amount of material added to the thermoplastic polymer was adjusted to maintain 0.75 vol % SWNTs in all composites. Based on the presence of clear van Hove singularities and UV−vis absorption at an aqueous SWNT concentration of 2 mg/mL, PVP was a better dispersant than aqueous SDS (Figure S2). Therefore, it was expected that PVP-SWNT (0.75 vol % SWNT) would result in a more uniform dispersion in the nanocomposites than those prepared from SDS-SWNT and that both types of functionalized SWNTs would result in better dispersion than pristine SWNTs.

https://doi.org/10.1021/acsomega.0c06174
ACS Omega 2021, 6, 10618−10628

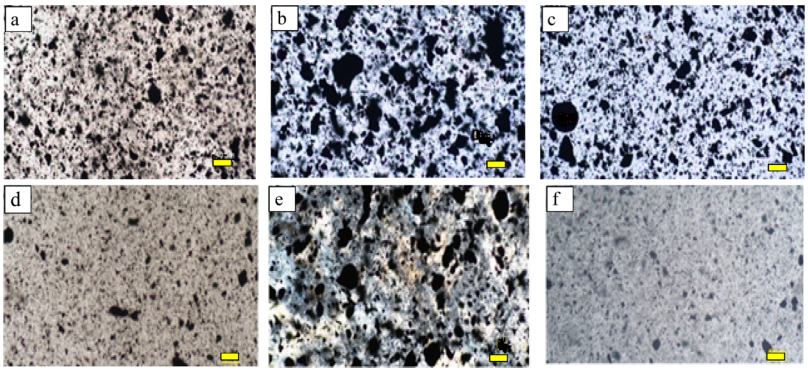

Figure 1. Optical microscopy images of nanocomposites prepared by different methods. RE method: (a) PP/SWNT, (b) PP/PVP-SWNT, and (c) PP/SDS-SWNT. Simplified SFD method: (d) PP/SWNT, (e) PP/PVP-SWNT, and (f) PP/SDS-SWNT (scale bars: 50 μm).

2.2. PP Nanocomposites. *2.2.1. Morphology.* Morphological characterization of nanocomposites using optical and scanning electron (SEM) microscopy was used to gain initial qualitative insights into the extent of SWNT aggregation in the nanocomposites prior to a more detailed assessment based on rheological and thermal behavior. Although the aqueous PVP-SWNT had the best dispersion, PVP-SWNT resulted in the worst dispersion in PP nanocomposites prepared by the previously developed RE method.[14] As shown in Figure 1, PP/PVP-SWNT contained numerous aggregates, many of which were greater than 50 μm in size. Based on the visual and spectroscopic assessment of the aqueous dispersion, these aggregates had to form either during RE or during melt processing. To test the hypothesis that the aggregate formation was due to capillary forces during vacuum drying, drops of aqueous PVP-SWNT and pristine SWNT dispersions were placed on glass slides and dried in a vacuum oven. The dried PVP/SWNTs had aggregates with diameters up to 300 μm, while the aggregates in the pristine SWNTs were <100 μm in spite of SWNTs' inherent hydrophobicity (Figure 2). While poorly dispersed SWNTs do not get more finely dispersed during drying, capillary forces can cause even uniformly dispersed SWNTs to undergo significant aggregation, even in the presence of a dispersion aide that provides steric hindrance.[11,30] However, the presence of the thermoplastic polymer and melt processing shear can provide some mitigation of aggregation tendencies; the aggregate size (Figure 1b) in the nanocomposites was smaller than that in the vacuum-dried dispersion. The SDS-SWNT nanocomposites prepared by the RE method (Figure 1b) showed aggregation similar to the pristine SWNTs, again highlighting that a uniform initial SWNT dispersion will not always provide the best results.

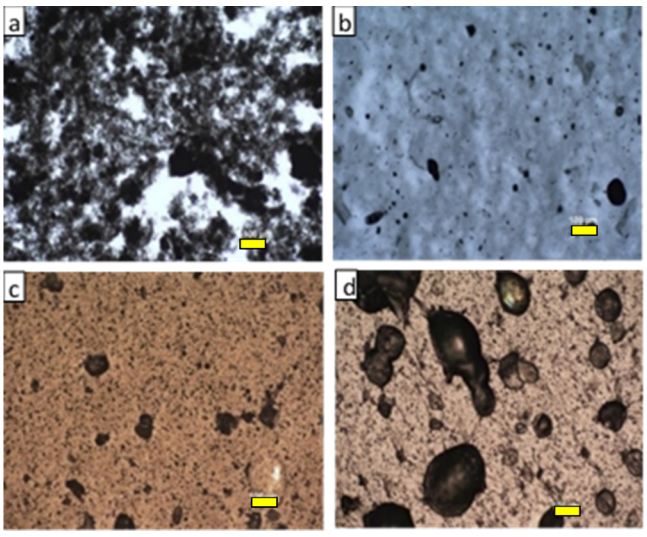

Figure 2. Optical microscopy images of aqueous dispersions before and after vacuum-drying. Before vacuum-drying: (a) SWNT/water dispersion and (b) PVP-SWNT/water dispersion. After vacuum-drying, (c) SWNT/water dispersion (d) PVP-SWNT/water dispersion (scale bars 100 μm). The vacuum-dried PVP-SWNT had much larger aggregates than the initial dispersion.

PP/SWNT, PP/PVP-SWNT, and PP/SDS-SWNT were also prepared using a low-cost SFD method in which droplets of the dispersion were sprayed into liquid nitrogen using a household spray bottle (such as a travel-size container for hair-spray) and the solidified water was removed by sublimation in a freeze-dryer. Similar to the RE method, the PVP-SWNT (Figure 1e) nanocomposites had larger and more numerous aggregates than the other two SFD nanocomposites. This suggests that the aggregation was not solely a function of capillary forces during drying. According to Flory–Huggins theory for polymer pair miscibility, the interactions among polymer molecules may be evaluated using the solubility parameters, which are determined from the dispersion forces, polar forces, and hydrogen bonding.[31,32] When two polymers have approximately equal solubility parameters, they tend to be miscible with each other. The solubility parameters for the polymers, PVP and PP, were calculated using Hoftyzer–van Krevelen method.[33,34] The calculated solubility parameter values for PVP and PP are 24.3 $(MPa)^{0.5}$ and 17 $(MPa)^{0.5}$, respectively (Table S1). Based on these parameters and the concentration of PVP in the composites, Flory–Huggins theory indicates that PVP and PP are immiscible. For SDS, the solubility parameter was found to be 19 $(MPa)^{0.5}$ using Fedors method, and the Flory–Huggins equation indicated SDS and PP should be miscible.[33] The presence of small aggregates in the PP/SDS-SWNT (Figure 1f) is therefore attributed to small aggregates in the initial SDS-SWNT dispersion. In contrast to the PVP-SWNT dispersion, the UV–vis spectra for SDS-SWNT lacked clear van Hove peaks (Figure S2). This indicates that the SWNTs were not individually dispersed. The fact that a poorer initial dispersion resulted in fewer aggregates, highlights the need to consider thermodynamic compatibility and dispersion state throughout the nanocomposite production process.

Based on optical microscopy (Figure 1), the PP/PVP-SWNT made by SFD only had slightly less aggregation than that made

https://doi.org/10.1021/acsomega.0c06174
ACS Omega 2021, 6, 10618–10628

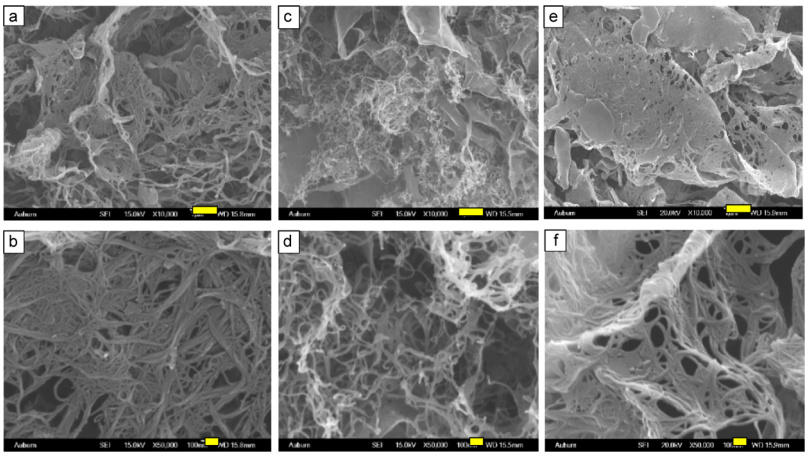

Figure 3. Representative SEM images of SFD dispersions at two magnifications: (a,b) SWNT, (c,d) PVP-SWNT, and (e,f) SDS-SWNT. Scale bars are 1 μm in the top row and 100 nm in the bottom row.

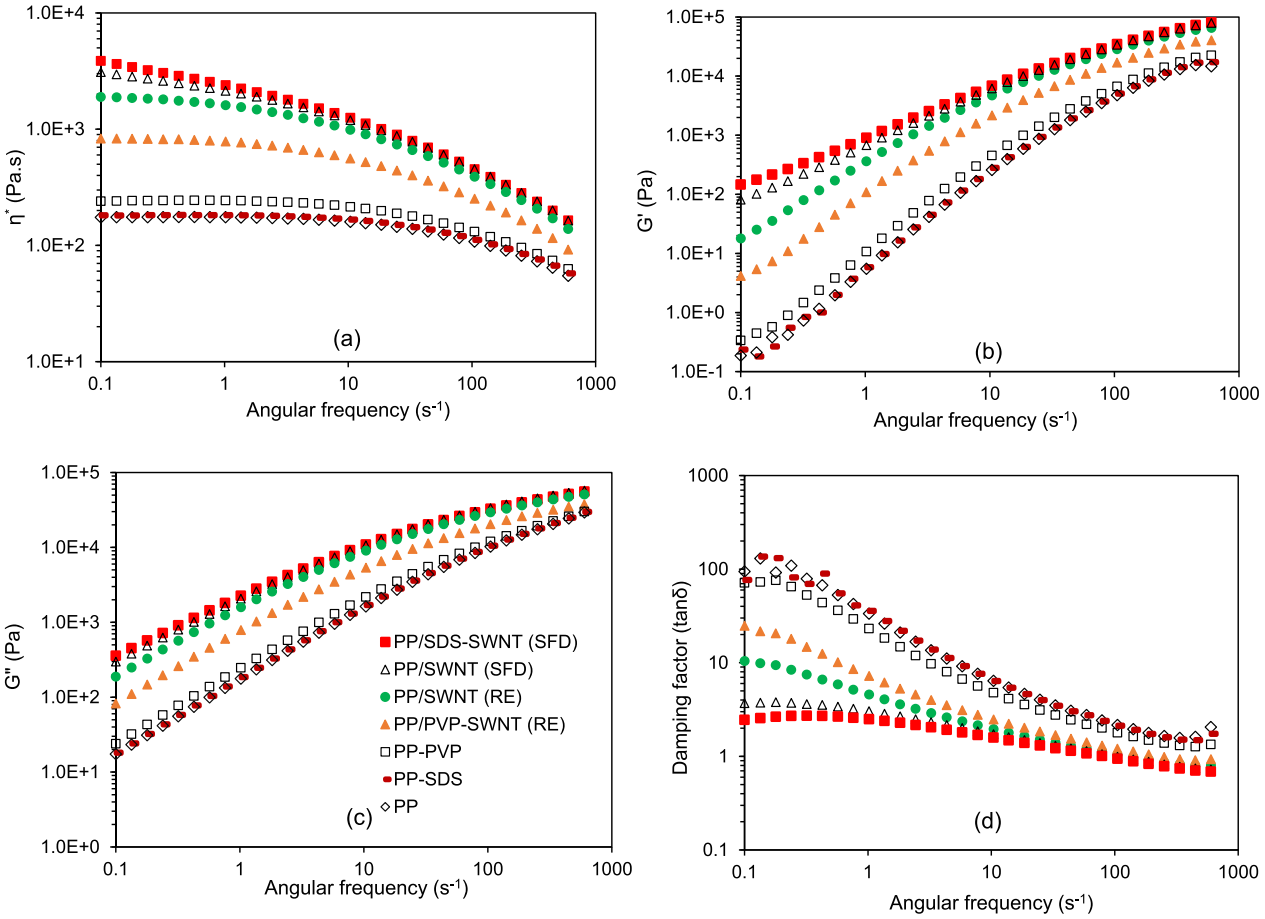

Figure 4. Rheology of PP and PP/SWNT nanocomposites. (a) Complex viscosity, (b) storage modulus, (c) loss modulus, and (d) damping factor as a function of angular frequency. Legends shown in (c) are the same for all figures. (Error bars smaller than symbols and <15%.)

by RE. However, the other two SFD nanocomposites had much finer dispersion than the corresponding RE nanocomposites. Notably, for the SFD nanocomposites the PP/SDS-SWNT which started from a uniform aqueous dispersion had (Figure 1e) a noticeably more uniform nanocomposite microstructure than pristine PP/SWNT which started from an aqueous dispersion of aggregates. This highlights that in the absence of incompatibility with the matrix, the finer initial dispersion results in the finer dispersion in the composite. Better SWNT dispersion in nanocomposites prepared via the SFD method compared to the RE method can be attributed to SFD removing the water through sublimation instead of evaporation. Sublimation avoids the capillary-force-induced aggregation associated with crossing the liquid−vapor phase transition. In addition, when the dispersion is quickly frozen in liquid nitrogen, a moving ice front creates space between the solute (SWNT) particles. Removal of the ice through sublimation

https://doi.org/10.1021/acsomega.0c06174
ACS Omega 2021, 6, 10618−10628

results in a porous structure[11] which can then be more easily intercalated by polymer chains during extrusion.[35,36]

In conventional freeze drying, a container of a dispersion is lyophilized; this results in large flakes or a three-dimensional aerogel structure. These larger materials can still be difficult to mix with a polymer during extrusion. In contrast, SFD enables lyophilization of individual droplets. This results in numerous porous particles that can be more easily mixed. SFD is of increasing interest in biotechnology, but the expense and size requirements of commercial spray-freeze dryers have inhibited exploring this process for nanocomposites. However, this research showed that similar structures could be obtained by using a household spray bottle to spray the dispersion into a container of liquid nitrogen and then lyophilizing the frozen particles. In this work, it was found that simply putting the dispersion in a consumer spray bottle, spraying it into a bowl-shaped Dewar of liquid nitrogen, and lyophilizing the granules in a standard freeze dryer provided the benefits of using a larger, more expensive commercial SFD albeit without precise control of droplet or ice granule size. As shown in Figure 3, the SFD method used in this research resulted in an open microstructure of small bundles. Representative images of the denser microstructure of evaporated dispersions are shown in Figure S3. The more porous structures in the SFD samples resulted in lower agglomerate strength and easier polymer melt infiltration during melt processing. While SEM images only show a small area, the bundle sizes appeared to be largest for SWNT and smallest for PVP-SWNT. This is consistent with the UV−vis spectra of the PVP-SWNT dispersion showing that it had the best initial dispersion state and further supports that the aggregation in the PP/PVP-SWNT nanocomposites was due to thermodynamic incompatibility. In previous work, SEM images of PP/SWNT nanocomposites have been shown to provide limited information about dispersion.[14] Similarly, in this study SEM images of the PP/SWNT and PP/SDS-SWNT nanocomposites were compared to see if the different dispersants resulted in distinct differences in SWNT bundle sizes. However, no noticeable differences were observed (Figure S4).

2.2.2. Rheology. Rheology provides a more sensitive assessment of nanocomposite microstructures than imaging methods. Even when image quantification methods are used, optical and scanning electron microscopy only probe small sample areas, while rheology probes milliliter volumes of samples. Small amplitude oscillatory shear (SAOS) was used to measure the complex viscosities η^*, storage moduli G', loss moduli G'', and damping factors ($\tan\delta = G''/G'$) of the nanocomposites. Figure 4 shows the range of properties that could be achieved. Comparison of PP, PP/PVP, and PP/SDS shows that the dispersant did not significantly modify the PP rheological properties. Comparison of PP/SWNT by RE and SFD shows that the SFD samples had higher complex viscosity and storage modulus at low frequencies where the behavior of the SWNTs dominates the response. This was likely due to the infiltration of polymer chains into the porous structure of the SFD SWNT. Typically, for a fixed concentration, both η^* and G' increase with increased nanomaterial dispersion; increased dispersion increases the fraction of polymer chains constrained in the interphase between the nanomaterial and the bulk polymer. The additional curves for PP/PVP-SWNT produced by RE and PP/SDS-SWNT produced by SFD show the two extremes of behavior. While PP/PVP-SWNT had higher complex viscosity and storage modulus than pure PP, the values were markedly lower than for PP/SWNT. This is consistent with PVP's lower thermodynamic compatibility with the matrix and the poorer dispersion observed in the optical images. On the other hand, PP/SDS-SWNT made by SFD had properties similar to pure PP/SWNT except at the lowest frequencies where it had higher values of η^* and G'.

The frequency dependence of G' and G'' provides further insights into the nanocomposites' microstructures. Both higher values of G' at low ω and lower slopes of G' versus ω typically indicate improved SWNT dispersion. Consistent with the values of η^*, PP/PVP-SWNT showed the smallest increase in G' relative to PP, and PP/SDS-SWNT had the largest increase in G' relative to PP (Figure 4b). The nearly 3 order of magnitude increase in G' at 0.75% SWNT highlights how much the inclusion of high aspect ratio nanomaterials can affect viscoelastic properties. At low frequencies, the PP chains exhibited nearly terminal behavior with $G' \propto \omega^{1.7}$. However, in the nanocomposites, the terminal behavior disappeared because the polymer chains were effectively restrained by the presence of SWNTs. The slopes of the low-frequency region decreased with improved SWNT dispersion; for the poorly dispersed PP/PVP-SWNT, $G' \propto \omega^{1.4}$, while for the well-dispersed PP/SDS-SWNT, $G' \propto \omega^{0.8}$. However, the fact that the curve did not become flat at low frequency indicates that the SWNTs were unable to form a completely percolated network and that some nanotubes still existed as large bundles.

The low-frequency dependence of G'' (Figure 4c) showed a similar trend to G'; however, the corresponding increase in the loss modulus of the nanocomposites was much lower than that of the storage modulus. The damping factor ($\tan\delta = G''/G'$) provides insight into the relative changes in G' and G'' and is shown in Figure 4d; it also provides information regarding the microstructure and interfacial interactions between the nanotubes and the PP matrix.[37] For all of the nanocomposites, $\tan\delta > 1$ at all frequencies; this highlights that the viscous nature of PP dominated the behavior. However, for the SFD nanocomposite samples, $\tan\delta \sim 1$ at $\omega \to 0$ due to the increased elastic nature of these nanocomposites at long time scales. Moreover, the flatness of the $\tan\delta$ versus ω curve for SDS-SWNT and pristine SWNT SFD nanocomposites indicates significant interfacial interactions with the matrix. In contrast, the steeper slope for PP/PVP-SWNT indicates less interfacial interaction and provides further evidence of poor thermodynamic compatibility.

2.2.3. Thermal Properties. SWNTs can improve the thermal stability of polymer matrices by stabilizing the polymer chains against thermal energy and reducing the transport of decomposition products.[38,39] In order to observe the thermal stabilizing effect of nanotubes, TGA was used to determine the temperature at 5% weight loss T_d and the temperature at which there was a maximum rate of weight loss T_1 (Table 1). The increase in the nanocomposite T_d and T_1 compared to that of neat PP was due to the stabilization of PP chains in the SWNT/polymer interphase and the reduced transport of evolved decomposition products caused by the presence of nanotubes.[38,39] A uniform SWNT dispersion leads to both a larger interphase volume and a more complex nanotube network; this results in the stabilization of more polymer chains and a reduction in the transport degradation products. For pure PP in nitrogen, T_d = 404 °C. SFD PP/SDS-SWNT showed the largest increase in thermal stability and had T_d = 442 °C. This is consistent with the rheological results showing that the SWNTs were better dispersed in this sample. Interestingly,

https://doi.org/10.1021/acsomega.0c06174
ACS Omega 2021, 6, 10618−10628

Table 1. Thermal Decomposition (T_d) and Temperature of Maximum Rate of Weight Loss (T_1) for Neat PP and Nanocomposites[a]

method	sample	T_d (°C)	T_1 (°C)
	PP	404	463
RE	PP/SWNT	435	470
	PP/PVP-SWNT	416	464
	PP/SDS-SWNT	424	472
SFD	PP/SWNT	435	474
	PP/PVP-SWNT	421	466
	PP/SDS-SWNT	442	477

[a]Rotary evaporation (RE), spray-freeze drying (SFD). (T_d and T_1 values are within the error range of ±1.5 °C).

both RE and SFD PP/SWNT had T_d = 435 °C even though the rheological results indicated that the SFD sample had a higher degree of dispersion. Consistent with SWNT dispersion affecting T_d, the poorly dispersed RE PP/PVP-SWNT only had T_d = 416 °C, while the slightly better dispersed SFD PP/PVP-SWNT had T_d = 421 °C. Comparing the derivative peaks, T_1 showed similar trends as the T_d values and supported that the SFD method resulted in better dispersion and more chain stabilization.

Differential scanning calorimetry (DSC) was used to understand the impacts of the composition and processing method on the polymers' melting temperature and crystallization. Table 2 provides the melting temperatures T_m, crystallization temperatures T_c, and crystallization kinetic parameters for the PP nanocomposites. For both the SFD and RE nanocomposites, T_m increased by only 2−4 °C. While this is consistent with SWNTs causing some restriction of polymer mobility, the lack of an observable trend and the ±1 °C experimental error inherent in DSC measurements suggest that any effects of SWNTs on T_m was insignificant. The presence of SWNTs was expected to result in an increase in T_c because the nanotubes act as heterogeneous nucleation sites.[40] For loading of 0.5 vol. %, Radhakrishnan et al. observed a 10 °C increase in T_c,[14] with 1 wt. % SWNTs. Bhattacharyya et al.[41] found an 11 °C increase in T_c, whereas Manchado et al. observed an increase of 5 °C.[16] In this work, for the RE nanocomposites, the smallest increases in T_c relative to PP were 8 and 10 °C for PP/PVP-SWNT and PP/SDS-SWNT, respectively. In contrast, PP/SWNT showed an increase of 14 °C resulting in T_c = 130 °C. The SFD nanocomposites had T_c ∼ 130 °C for both PP/SWNT and PP/SDS-SWNT. These results generally suggest that poorer dispersion results in a smaller increase in T_c, but other factors such as the presence of an additive also seem to be affecting the crystallization temperature.

Table 2. Thermal Transitions in PP Nanocomposites[a]

method	sample	T_c (°C)	T_m (°C)	$t_{1/2}$ (s) (at 133 °C)	ΔE_a (kJ/mol)
	PP	116	162	259	344
RE	PP/SWNT	130	165	32	204
	PP/PVP-SWNT	124	164	131	337
	PP/SDS-SWNT	126	164	108	311
SFD	PP/SWNT	131	165	29	208
	PP/SDS-SWNT	132	166	22	137

[a]Error is ±1 °C for T_m and T_c.

Analysis of the isothermal crystallization kinetics further aided in understanding the effects of pre-processing methods and functionalization on PP nanocomposites. The isothermal crystallization kinetics were determined using the Avrami equation (eq 1), which relates the crystallized fraction of polymer x to the overall rate constant of crystallization k, time t, and Avrami exponent n.

$$x = 1 - \exp(-kt^n) \tag{1}$$

$$\ln[-\ln(1 - x_t)] = \ln k + n \ln t \tag{2}$$

By plotting $\ln[-\ln(1 - x_t)]$ versus $\ln t$, the values of the Avrami exponent and crystallization rate constant were obtained from its slope and intercept. The activation energy E_a of crystallization was evaluated using an Arrhenius-type equation and determining the slope of a $\ln k$ versus $1/T$ plot

$$\ln k = \ln k_0 - \frac{E_a}{R \cdot T} \tag{3}$$

where k_0 is the frequency factor and R is the gas constant. The half time of crystallization $t_{1/2}$ was obtained from the modified form of eq 2

$$t_{1/2} = \left(\frac{\ln 2}{k}\right)^{1/n} \tag{4}$$

Table 2 shows the $t_{1/2}$ and E_a values for neat PP and its nanocomposites. Consistent with nanotubes acting as heterogeneous nucleation sites, the nanocomposites' crystallization half times were 10−50% of the $t_{1/2}$ = 259 s for pure PP. The $t_{1/2}$ trend was generally in accordance with the morphological and rheological results, with the SFD samples having a faster crystallization rate than any of the RE samples. However, the difference between RE and SFD crystallization kinetics of PP/SWNT was negligible. The value of E_a is also affected by the presence of heterogeneous nucleation sites. However, the effect of nanotubes on E_a is more complex because while the presence of nucleation sites tends to reduce E_a, lower polymer chain mobility resulting from increased viscosity tends to increase E_a.[15,42] In this work, E_a followed a similar trend as $t_{1/2}$. For neat PP, E_a = 344 kJ/mol, while the values for RE and SFD PP/SWNT were much lower at 204 and 208 kJ/mol, respectively. However, for SFD PP/SDS-SWNT, E_a was only 137 kJ/mol compared to 311 kJ/mol for RE PP/SDS-SWNT.

2.3. EVOH Nanocomposites. To further explore the utility of the SFD method and verify that the poor results for PP/PVP-SWNT were due to poor compatibility between PP and PVP, EVOH/PVP-SWNT nanocomposites were prepared. In contrast to PP, the EVOH grade used in this research had favorable interactions with PVP due to a 52 mol % vinyl alcohol content. This compatibility is due to hydrogen bonding between the proton-accepting carbonyl moiety in PVP's pyrrolidone ring and the vinyl alcohol's hydroxyl side group.[43−46] PVP's compatibility with EVOH (Table S1) was experimentally confirmed by using DSC to characterize the glass transition temperature T_g.[31] Compatible polymer blends have a single T_g peak at a temperature between the T_g's of the individual components. The glass transition temperatures of EVOH and PVP are 49 and 164 °C, respectively. Therefore, the single peak at T_g = 79 °C for PVP-EVOH blends is a confirmation of thermodynamic compatibility (Figure S5).

2.3.1. Morphology. As shown in Figure 5a,b optical microscopy images of EVOH/SWNT and EVOH/PVP-

https://doi.org/10.1021/acsomega.0c06174
ACS Omega 2021, 6, 10618−10628

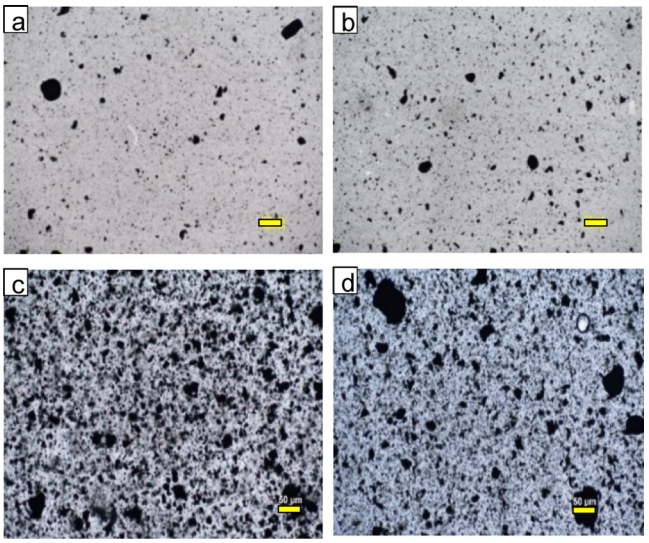

Figure 5. Optical images for EVOH nanocomposites extruded at 190 °C, 100 rpm, and 30 min (0.75 vol % SWNT). (a) EVOH/SWNT (SFD), (b) EVOH/PVP-SWNT (SFD), (c) EVOH/SWNT (RE), and (d) EVOH/PVP-SWNT (RE) (scale bars: 50 μm).

SWNT nanocomposites prepared through SFD showed a uniform dispersion state with only fewer aggregates than those made by SFD. The presence of PVP still resulted in some increased aggregation for the RE composites; this is likely due to aggregation induced by capillary forces. However, for SFD EVOH/PVP-SWNT, increased aggregation was not observed. In fact, SEM images of both EVOH/SWNT and EVOH/PVP-SWNT nanocomposites showed uniformly dispersed SWNT bundles without any noticeable differences between them (Figure 6). This supports that the aggregation in the

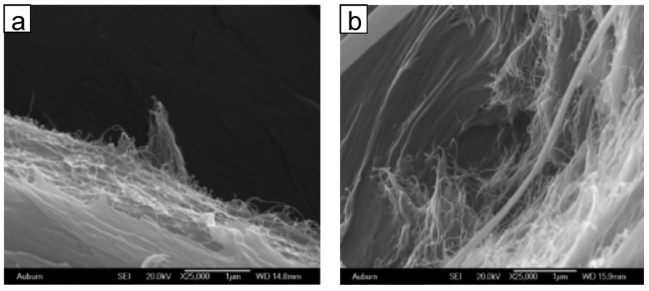

Figure 6. SEM images of (0.75 vol %) EVOH nanocomposites through SFD extruded at 190 °C, 100 rpm, and 30 min. (a) EVOH/SWNT and (b) EVOH/PVP-SWNT (scale bars: 1 μm).

corresponding PP composite was due to thermodynamic incompatibility. The RE EVOH nanocomposites were not further characterized due to the large aggregates compared to the SFD EVOH composites.

2.3.2. Rheology. The rheological results confirmed that the presence of PVP aided the SWNT dispersion in EVOH. The low shear viscosity of EVOH/PVP-SWNT was twice that of EVOH/SWNT and five times that of EVOH or EVOH/PVP. Similar differences were seen in G'. In fact, unlike the PP nanocomposites, the SWNTs in EVOH/PVP-SWNT were so well-dispersed that at low frequencies, G' was nearly flat, indicating the initial onset of SWNT network formation (Figure 7a). The differences in nanocomposite microstructure are further highlighted in the Cole−Cole plot shown in Figure 8. Neat EVOH and EVOH/PVP showed a linear relationship between G' and G'', typical of polymer melts. While all nanocomposites showed a deviation from linearity, the greatest deviation was observed for EVOH/PVP-SWNT, indicating more solid-like behavior due to the presence of a highly complex microstructure.

2.3.3. Thermal Properties. EVOH exhibited the multistep decomposition behavior due to its two structural components. The vinyl component decomposed below 400 °C, and the more stable ethylene component decomposed above 400 °C (Figure S6). The thermal stability of the EVOH nanocomposites was measured in terms of the temperatures at which there was a maximum rate of weight loss for these two components. The peak temperatures T_1 and T_2 (Figure S6b) corresponding to the respective decomposition of the vinyl and ethylene components are tabulated in Table 3. The stabilizing effect of SWNTs on the vinyl component of EVOH is evident from the 12 °C increase in T_1 for EVOH/PVP-SWNT and the 9 °C increase for EVOH/SWNT. These results are consistent with greater dispersion and more favorable interfacial interactions in EVOH/PVP-SWNT. However, T_2, which largely corresponded to ethylene decomposition, was not affected by the presence of SWNTs. This might be due to the poor interaction of PVP with EVOH's ethylene component. Similar behavior has been reported for polyethylene−MWNT nanocomposites where the temperature corresponding to the maximum rate of weight loss was unaffected by the addition of different concentrations of MWNTs.[47]

Table 3 also summarizes the thermal transitions for the nanocomposites. As for PP/SWNT, differences in the melting temperature were negligible. A slight increase from 47.8 to 51.0 °C was seen for the glass transition temperature; this suggests that the nanotubes had a slight impact on polymer chain mobility at the interphase. In contrast to the PP nanocomposites, the presence of SWNTs in EVOH only slightly affected the crystallization behavior, even though the nanotubes were well-dispersed based on morphological and rheological measurements. The crystallization temperature T_c was only 2−3 °C higher than the 138 °C value for EVOH. Figure S7 shows an example of the DSC curves. However, the percent crystallinity X_c was lower for the EVOH nanocomposites than for the pure EVOH. The presence of SWNTs hindered the regular packing of the EVOH chains into crystal lattices, eventually leading to the diminished crystallite size. The values of X_c shown in Table 3 were calculated using eq 5

$$X_c = \frac{\Delta H_m}{\Delta H_{m,EVOH}(1 - W_f)} \times 100 \quad (5)$$

where W_f is weight fraction of nanotubes, ΔH_m is the enthalpy of melting of the sample, and $\Delta H_{m,EVOH}$ is the enthalpy of melting when the sample is 100% crystalline, which was taken as 128.1 J/g.[48] A similar reduction in the crystallinity of EVOH caused by the incorporation of nanofillers has also been reported for EVOH/graphene oxide nanocomposites.[48]

3. CONCLUSIONS

RE and SFD as pre-processing techniques in conjunction with non-covalent functionalization were investigated for their effects on SWNT dispersion for composites prepared in a small conical twin screw extruder with a recirculation channel. It is likely that better dispersion could be achieved using an extruder with distributive and dispersive mixing elements. The

https://doi.org/10.1021/acsomega.0c06174
ACS Omega 2021, 6, 10618−10628

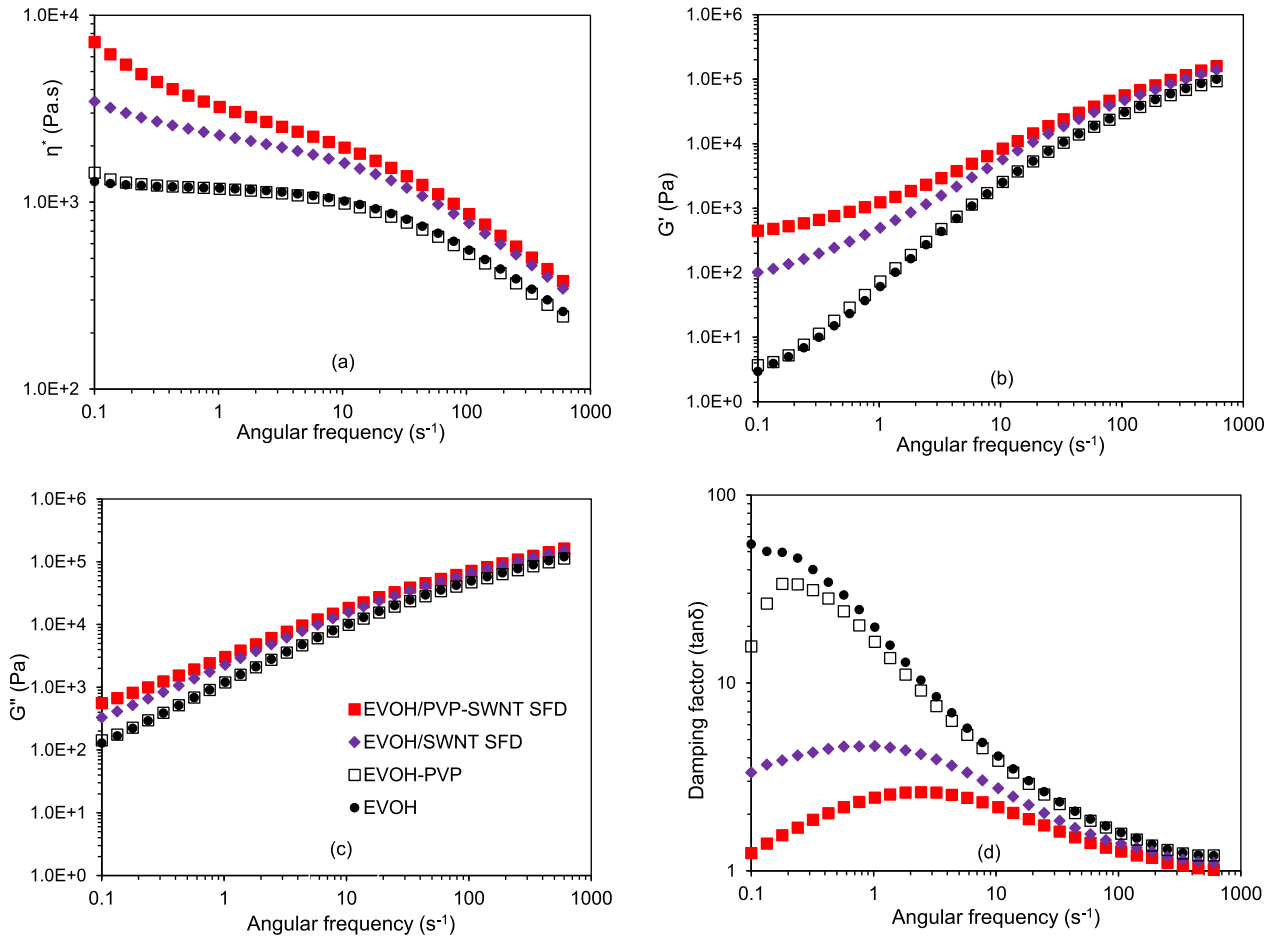

Figure 7. Rheology of EVOH and EVOH/SWNT nanocomposites. (a) Complex viscosity, (b) storage modulus, (c) loss modulus, and (d) damping factor as a function of angular frequency (error bars: < 15%). Legends shown in (c) are the same for all figures.

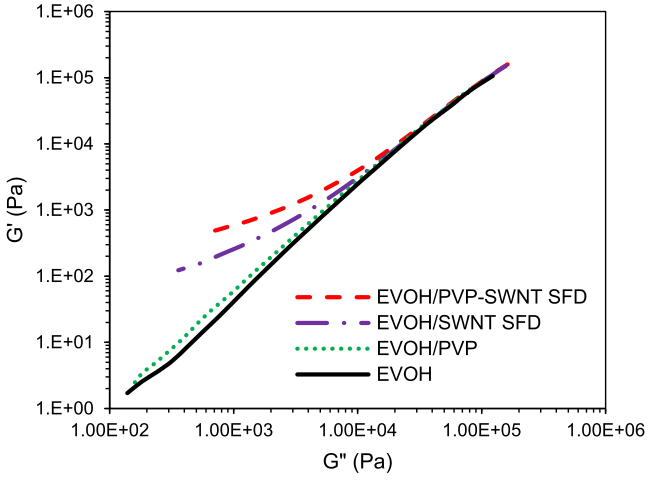

Figure 8. Cole−Cole plot for EVOH nanocomposites. Lines used to guide the eye.

results of this research demonstrate that a simplified SFD method facilitates SWNT dispersion. SFD of an aggregated aqueous dispersion of pristine SWNTs resulted in porous granules that could be sufficiently well-dispersed in polymers to alter both rheological and thermal properties. This research also highlights that the initial SWNT dispersion state is not the sole governing factor in achieving uniform nanocomposites, and thermodynamic compatibility of the dispersion aide and polymer matrix must also be considered. PVP is generally known as a low-cost, easy to use SWNT dispersion aide, and it enabled aqueous dispersions exhibiting the van Hove peaks indicative of individual dispersion. However, the PP/PVP-SWNT nanocomposites had large aggregates due to PVP's thermodynamic incompatibility with the matrix, while PVP-SWNT were relatively well-dispersed in EVOH.

4. EXPERIMENTAL SECTION

4.1. Materials. The SWNTs used in this research were manufactured through the CoMoCat process and were obtained from SouthWest Nano Technologies (now

Table 3. Thermal Properties of EVOH Nanocomposites

sample	T_1 (°C)	T_2 (°C)	T_g (°C)	T_m (°C)	T_c (°C)	H_c (J/g)	H_m (J/g)	X_c (%)
EVOH	367	459	47.8	158	138	59.9	54.0	42.1
EVOH/SWNT (SFD)	376	458	51.0	157	140	50.1	46.5	36.6
EVOH/PVP-SWNT (SFD)	379	458	51.0	158	141	53.6	49.0	37.0

https://doi.org/10.1021/acsomega.0c06174
ACS Omega 2021, 6, 10618−10628

CHASM, Norman, OK). SWNT grades CG200 (Lot L04 and L14) and CG300 (Lot L3) were used for the PP and EVOH nanocomposites, respectively. These SWNT batches were previously characterized using the following methods.[21,49] The purity was determined using a TA Instruments (New Castle, DE) Q50 TGA. With air as the gas, the temperature was ramped from room temperature to 800 °C at 10 °C/min with a 20 min hold at 120 °C to remove moisture and a 45 min hold at 800 °C. The percentage of actual SWNT, non-SWNT carbon, and the catalyst was calculated using the method recommended by Sigma-Aldrich.[50] Nanotube lengths and diameters were measured on functionalized SWNTs using a Pacific Nanotechnology Inc. (Santa Clara, CA) Nano-R atomic force microscope.[21,49] Aspect ratios were based on images obtained from dried samples of SWNTs covalently functionalized with dodecyl groups in chloroform or SWNTs noncovalently functionalized with lyophilized salmon sperm double-stranded DNA.[21,49,51] Raman spectra were obtained using both 514 and 785 nm lasers on a Renishaw inVia Raman microscope (Hoffman Estates, IL) using a Leica 50× long (0.75 NA) objective. The spectra were an accumulation of 10 runs with an exposure time of 10 s for each run. All batches had similar properties of density 1.45 g/cm^3 and D/G ratio of 0.1 with an average aspect ratio of ∼460. Both CG300 and CG200 are enriched in metallic SWNTs; CG300 had a higher purity of 95% SWNTs compared to 85% for CG200. PVP (M_w = 40,000) and SDS were purchased from Sigma-Aldrich (St. Louis, MO). PP (melt flow index = 12, M_n = 63,000) was obtained as flakes from Total Petrochemicals (Houston, TX). EVAL G176 EVOH (48 mol % ethylene) was obtained from Kuraray America (Houston, TX). Irganox 225B and Irgastab FS301 were obtained from BASF (Tarrytown, NY) and added to PP prior to extrusion to improve polymer thermo-oxidative stability.

4.2. Non-covalent Functionalization of SWNTs. Noncovalent SWNT functionalization with PVP was performed in water. While early work on SWNT/PVP initially involved first dispersing the SWNTs in SDS,[25] dispersion of individual SWNTs in water could also be achieved without this initial step.[52] A 2 mg/mL aqueous PVP stock solution was prepared by magnetically stirring the required quantities of PVP in distilled water for 10 min; SWNTs were added to a portion of the stock solution at a 1:1 ratio (by weight) of SWNT/PVP. The mixture was bath-sonicated for 20 min and then ultrasonicated using a SONICS Vibra-cell tip sonicator for 30 min at 60% amplitude (∼60 W), with cycles of 5 s on and 3 s off. A similar procedure was used for SWNT functionalization using SDS. A control sample of 2 mg/mL aqueous SWNT dispersion without any polymer or surfactant was also prepared using the same sonication treatment for comparison.

4.3. Pre-processing Methods. The details of the RE method are fully described by Radhakrishnan et al. (2010).[14] In short, the solid polymer (PP or EVOH) was initially mixed with 2 mg/mL aqueous dispersion of non-covalently functionalized or pristine SWNTs using magnetic stirring for 10 min. The polymer mass and SWNT dispersion volume were measured in order to get 0.75 vol % (1.2 wt %) SWNT in the final nanocomposite. The water was evaporated at 100 °C under vacuum in a Buchi RE-121 rotary evaporator. The rotary evaporator provided a continuous movement of the mixture during water evaporation, finally producing the polymer with a uniform coating of SWNTs. To further assure complete water removal, the SWNT-coated polymer was vacuum dried overnight at 80 °C for 6 h.

The simplified SFD method used the same type of dispersion but consisted of using a consumer spray bottle (such as a travel bottle for hair spray) to spray 2 mg/mL aqueous dispersions of the noncovalently functionalized or pristine SWNTs into a container with liquid nitrogen. The fine droplets obtained from the spray nozzle formed a frozen slurry in the container, which was kept in suspension using magnetic stirring. This slurry was then transferred to freeze-drying flasks and lyophilized for 48 h using a Labconco 4.5 Freezone. The resulting samples were further dried at 80 °C under vacuum for 6 h to remove any residual moisture. These samples were then blended with the polymer by manually shaking in a vial for 1 min just prior to extrusion.

4.4. Nanocomposite Preparation. The volume-based concentration of SWNTs in the nanocomposites was calculated from the mass fractions using ρ_{SWNT} = 1.45 g/cm^3, ρ_{PP} = 0.90 g/cm^3, and ρ_{EVOH} = 1.12 g/cm^3. The estimated critical volume fraction for percolation of individual SWNT adducts was 0.35% < ϕ_c < 0.70%. Therefore, a concentration of 0.75 vol % SWNTs (∼1.2 wt %) was chosen with the expectation that this would be sufficient for percolation. The actual amount of material added to the polymer was adjusted to account for the presence or absence of noncovalent functionalization.

The pre-processed samples were extruded using a Haake Minilab counter-rotating twin screw extruder. The advantages of using the Minilab extruder were that it required a very low volume of materials (∼5 cm^3) and that the availability of a back channel allowed for the material recirculation through the barrel until the desired level of mixing was achieved. However, since the MiniLab has conical feeder screws without any mixing elements, dispersion requires longer times than on a traditional twin-screw extruder. Based on a previous work,[15] melt processing conditions of 190 °C and 100 rpm for 30 min were chosen for the PP and PP nanocomposite extrusion; the EVOH and EVOH nanocomposites were processed under the same conditions. The EVOH was used as received; however, since PP was not fully stabilized, Irganox 225B and Irgastab FS301 were dry-mixed and added to the pre-processed polymer samples at 0.25 and 0.15 wt %, respectively, to improve polymer thermo-oxidative stability during processing.

4.5. Characterization. *4.5.1. UV−Vis Spectroscopy.* A Thermo Scientific (Waltham, MA) NanoDrop 2000c UV−visible spectrophotometer was used to measure the absorbance of the noncovalently functionalized SWNTs. Scans were acquired at room temperature with a 1 mm path length from 190 to 840 nm with a 1 nm resolution.

4.5.2. Optical Microscopy. A Nikon (Melville, NY) Eclipse 80I optical microscope was used to image the dispersions and nanocomposites. The extruded nanocomposite samples were melt pressed onto glass microscope slides at 190 °C. Dried SWNT samples were directly prepared on microscope slides. A 20× objective (0.45 NA) and 2× magnification before the camera (translating to an effective magnification of 40×) were used to image the samples.

4.5.3. Scanning Electron Microscopy. SEM images were obtained using a JEOL (Tokyo, Japan) 7000-F field-emission scanning electron microscope; dried SWNT samples and polymer nanocomposite films were sputter-coated with gold before taking images.

4.5.4. Differential Scanning Calorimetry. Melting and crystallization temperatures of PP and EVOH were measured

https://doi.org/10.1021/acsomega.0c06174
ACS Omega 2021, 6, 10618−10628

on a TA Instruments (New Castle, DE) Q100 differential scanning calorimeter at a scan rate of 10 °C/min over a temperature range of 20−200 °C, using aluminum pans with lids. A heat−cool−heat cycle was performed to ensure the melting of all crystallites and to remove thermal history. The cycle consisted of the following steps: (1) heating at 10 °C/min to 200 °C followed by 5 min hold, (2) cooling at 10 °C/min to 20 °C with 5 min hold, and (3) heating at 10 °C/min to 200 °C. Isothermal crystallization studies for PP were performed by heating the sample to 200 °C at 10 °C/min with an isothermal hold of 5 min to ensure the melting of all crystallites, followed by rapid cooling at 100 °C/min to the desired crystallization temperature and holding isothermally for 30 min.

4.5.5. Thermogravimetric Analysis. Thermal stability was characterized using a TA Instruments (New Castle, DE) Q5000 thermal gravimetric analyzer (TGA). All TGA tests occurred under a constant nitrogen balance protection with a flow rate of 10 cm^3/min and a sample gas (nitrogen) flow rate of 25 cm^3/min. Samples were heated with a ramp rate of 10 °C/min to 120 °C. They were then held isothermally at 120 °C to ensure residual moisture removal. Samples were again ramped to 800 °C at 10 °C/min followed by an isothermal hold for 45 min. A sample size of ∼20 mg was used for every TGA test to avoid any potential deviations in heat flow or accuracy associated with the sample size.

4.5.6. Rheology. SAOS measurements were performed at 200 °C using 25 mm parallel plates on an Anton Paar (Ashland, VA) MCR 301 rotational rheometer equipped with a CTD 450 convection oven. For each sample, an amplitude sweep was used to determine the limit of the linear viscoelastic regime (LVR) based on the strain at which the storage modulus is 95% of the initial plateau values. Frequency sweeps between 0.1 and 600 s^{-1} were performed at percent strains well within, and typically an order of magnitude lower, than the LVR limit.

■ ASSOCIATED CONTENT

Supporting Information

The Supporting Information is available free of charge at https://pubs.acs.org/doi/10.1021/acsomega.0c06174.

TGA plots for PVP-SWNT and SDS-SWNT; UV-vis spectra of SWNT, SDS-SWNT, and PVP/SWNT; calculated solubility parameters; SEM images of melt-extruded PP nanocomposites PP/SWNT and PP/SDS-SWNT nanocomposites; DSC thermograms for PVP, EVOH, and EVOH/PVP blend; TGA curves for neat EVOH and 0.75 vol.% EVOH and neat PP and 0.75 vol.% PP nanocomposites; DSC thermograms showing crystallization peaks of EVOH nanocomposites; and DSC thermograms for neat PP and 0.75 vol.% PP nanocomposites (PDF)

■ AUTHOR INFORMATION

Corresponding Author

Virginia A. Davis − *Department of Chemical Engineering, Auburn University, Auburn, Alabama 36849, United States;* orcid.org/0000-0003-3126-3893; Email: davisva@auburn.edu

Author

Mahesh Parit − *Department of Chemical Engineering, Auburn University, Auburn, Alabama 36849, United States*

Complete contact information is available at: https://pubs.acs.org/10.1021/acsomega.0c06174

Notes

The authors declare no competing financial interest.

■ ACKNOWLEDGMENTS

The authors thank Sarah Grace Simpson for providing assistance in making nanocomposites. The National Science Foundation award number EPS-0814103 is acknowledged for funding.

■ REFERENCES

(1) Kayatin, M. J.; Davis, V. A. Viscoelasticity and shear stability of single-walled carbon nanotube/unsaturated polyester resin dispersions. *Macromolecules* **2009**, *42*, 6624−6632.

(2) McNally, T.; Pötschke, P.; Halley, P.; Murphy, M.; Martin, D.; Bell, S. E. J.; Brennan, G. P.; Bein, D.; Lemoine, P.; Quinn, J. P. Polyethylene multiwalled carbon nanotube composites. *Polymer* **2005**, *46*, 8222−8232.

(3) Baughman, R. H.; Zakhidov, A. A.; de Heer, W. A. Carbon nanotubes–the route toward applications. *Science* **2002**, *297*, 787−792.

(4) Che, J.; Çagin, T.; Goddard, W. A., III Thermal conductivity of carbon nanotubes. *Nanotechnology* **2000**, *11*, 65.

(5) Hone, J.; Whitney, M.; Piskoti, C.; Zettl, A. Thermal conductivity of single-walled carbon nanotubes. *Phys. Rev. B: Condens. Matter Mater. Phys.* **1999**, *59*, R2514.

(6) Krishnan, A.; Dujardin, E.; Ebbesen, T. W.; Yianilos, P. N.; Treacy, M. M. J. Young's modulus of single-walled nanotubes. *Phys. Rev. B: Condens. Matter Mater. Phys.* **1998**, *58*, 14013.

(7) Walters, D. A.; Ericson, L. M.; Casavant, M. J.; Liu, J.; Colbert, D. T.; Smith, K. A.; Smalley, R. E. Elastic strain of freely suspended single-wall carbon nanotube ropes. *Appl. Phys. Lett.* **1999**, *74*, 3803−3805.

(8) Yu, M.-F.; Files, B. S.; Arepalli, S.; Ruoff, R. S. Tensile loading of ropes of single wall carbon nanotubes and their mechanical properties. *Phys. Rev. Lett.* **2000**, *84*, 5552.

(9) Kim, P.; Shi, L.; Majumdar, A.; McEuen, P. Thermal transport measurements of individual multiwalled nanotubes. *Phys. Rev. Lett.* **2001**, *87*, 215502.

(10) Davis, V. A.; Green, M. J. Controlling and characterizing anisotropic nanomaterial dispersion. *Nanotechnol. Commer.* **2017**, 65−99.

(11) Khoshkava, V.; Kamal, M. R. Effect of drying conditions on cellulose nanocrystal (CNC) agglomerate porosity and dispersibility in polymer nanocomposites. *Powder Technol.* **2014**, *261*, 288−298.

(12) Khoshkava, V.; Kamal, M. R. Effect of surface energy on dispersion and mechanical properties of polymer/nanocrystalline cellulose nanocomposites. *Biomacromolecules* **2013**, *14*, 3155−3163.

(13) Haggenmueller, R.; Fischer, J. E.; Winey, K. I. Single wall carbon nanotube/polyethylene nanocomposites: Nucleating and templating polyethylene crystallites. *Macromolecules* **2006**, *39*, 2964−2971.

(14) Radhakrishnan, V. K.; Davis, E. W.; Davis, V. A. Influence of initial mixing methods on melt-extruded single-walled carbon nanotube−polypropylene nanocomposites. *Polym. Eng. Sci.* **2010**, *50*, 1831−1842.

(15) Radhakrishnan, V. K. Structure−Processing−Property interrelationships of vapor grown carbon nanofiber, single-walled carbon nanotube and functionalized single-walled carbon nanotube−polypropylene nanocomposites. Dissertation, Auburn University, 2010.

(16) Manchado, M. A. L.; Valentini, L.; Biagiotti, J.; Kenny, J. M. Thermal and mechanical properties of single-walled carbon nanotubes−polypropylene composites prepared by melt processing. *Carbon* **2005**, *43*, 1499−1505.

(17) Dondero, W. E.; Gorga, R. E. Morphological and mechanical properties of carbon nanotube/polymer composites via melt compounding. *J. Polym. Sci., Part B: Polym. Phys.* **2006**, *44*, 864−878.

(18) Fornes, T. D.; Baur, J. W.; Sabba, Y.; Thomas, E. L. Morphology and properties of melt-spun polycarbonate fibers containing single-and multi-wall carbon nanotubes. *Polymer* **2006**, *47*, 1704−1714.
(19) Lee, S. H.; Cho, E.; Jeon, S. H.; Youn, J. R. Rheological and electrical properties of polypropylene composites containing functionalized multi-walled carbon nanotubes and compatibilizers. *Carbon* **2007**, *45*, 2810−2822.
(20) Zhang, Q.; Rastogi, S.; Chen, D.; Lippits, D.; Lemstra, P. J. Low percolation threshold in single-walled carbon nanotube/high density polyethylene composites prepared by melt processing technique. *Carbon* **2006**, *44*, 778−785.
(21) Kayatin, M. J.; Davis, V. A. In situ polymerization functionalization of single-walled carbon nanotubes with polystyrene. *J. Polym. Sci., Part A: Polym. Chem.* **2013**, *51*, 3716−3725.
(22) Garg, A.; Sinnott, S. B. Effect of chemical functionalization on the mechanical properties of carbon nanotubes. *Chem. Phys. Lett.* **1998**, *295*, 273−278.
(23) Islam, M. F.; Rojas, E.; Bergey, D. M.; Johnson, A. T.; Yodh, A. G. High weight fraction surfactant solubilization of single-wall carbon nanotubes in water. *Nano Lett.* **2003**, *3*, 269−273.
(24) Moore, V. C.; Strano, M. S.; Haroz, E. H.; Hauge, R. H.; Smalley, R. E.; Schmidt, J.; Talmon, Y. Individually suspended single-walled carbon nanotubes in various surfactants. *Nano Lett.* **2003**, *3*, 1379−1382.
(25) O'Connell, M. J.; Boul, P.; Ericson, L. M.; Huffman, C.; Wang, Y.; Haroz, E.; Kuper, C.; Tour, J.; Ausman, K. D.; Smalley, R. E. Reversible water-solubilization of single-walled carbon nanotubes by polymer wrapping. *Chem. Phys. Lett.* **2001**, *342*, 265−271.
(26) Ramasubramaniam, R.; Chen, J.; Liu, H. Homogeneous carbon nanotube/polymer composites for electrical applications. *Appl. Phys. Lett.* **2003**, *83*, 2928−2930.
(27) Bhattacharyya, A. R.; Pötschke, P.; Abdel-Goad, M.; Fischer, D. Effect of encapsulated SWNT on the mechanical properties of melt mixed pA12/swnt composites. *Chem. Phys. Lett.* **2004**, *392*, 28−33.
(28) Chen, J.; Liu, H.; Weimer, W. A.; Halls, M. D.; Waldeck, D. H.; Walker, G. C. Noncovalent engineering of carbon nanotube surfaces by rigid, functional conjugated polymers. *J. Am. Chem. Soc.* **2002**, *124*, 9034−9035.
(29) Bose, S.; Khare, R. A.; Moldenaers, P. Assessing the strengths and weaknesses of various types of pre-treatments of carbon nanotubes on the properties of polymer/carbon nanotubes composites: A critical review. *Polymer* **2010**, *51*, 975−993.
(30) Thill, A.; Spalla, O. Aggregation due to capillary forces during drying of particle submonolayers. *Colloids Surf., A* **2003**, *217*, 143−151.
(31) Krause, S.; Compatibility, P.-P. *Polymer Blends 1*; Academic Press: New York, 1978.
(32) Barton, A. F. M. Solubility parameters. *Chem. Rev.* **1975**, *75*, 731−753.
(33) Van Krevelen, D. W.; Te Nijenhuis, K. *Properties of polymers: Their correlation with chemical structure; their numerical estimation and prediction from additive group contributions*; Elsevier, 2009.
(34) Li, L.; Jiang, Z.; Xu, J.; Fang, T. Predicting poly (vinyl pyrrolidone)'s solubility parameter and systematic investigation of the parameters of electrospinning with response surface methodology. *J. Appl. Polym. Sci.* **2014**, *131*, 40304.
(35) Ben Azouz, K.; Ramires, E. C.; Van den Fonteyne, W.; El Kissi, N.; Dufresne, A. Simple method for the melt extrusion of a cellulose nanocrystal reinforced hydrophobic polymer. *ACS Macro Lett.* **2011**, *1*, 236−240.
(36) Maugey, M.; Neri, W.; Zakri, C.; Derré, A.; Pénicaud, A.; Noé, L.; Chorro, M.; Launois, P.; Monthioux, M.; Poulin, P. Substantial improvement of nanotube processability by freeze-drying. *J. Nanosci. Nanotechnol.* **2007**, *7*, 2633−2639.
(37) Xu, D.-H.; Wang, Z.-G.; Douglas, J. F. Influence of carbon nanotube aspect ratio on normal stress differences in isotactic polypropylene nanocomposite melts. *Macromolecules* **2008**, *41*, 815−825.
(38) Marosfői, B. B.; Szabo, A.; Marosi, G.; Tabuani, D.; Camino, G.; Pagliari, S. Thermal and spectroscopic characterization of polypropylene-carbon nanotube composites. *J. Therm. Anal. Calorim.* **2006**, *86*, 669−673.
(39) Kashiwagi, T.; Grulke, E.; Hilding, J.; Harris, R.; Awad, W.; Douglas, J. Thermal degradation and flammability properties of poly (propylene)/carbon nanotube composites. *Macromol. Rapid Commun.* **2002**, *23*, 761−765.
(40) Valentini, L.; Biagiotti, J.; López-Manchado, M. A.; Santucci, S.; Kenny, J. M. Effects of carbon nanotubes on the crystallization behavior of polypropylene. *Polym. Eng. Sci.* **2004**, *44*, 303−311.
(41) Bhattacharyya, A. R.; Sreekumar, T. V.; Liu, T.; Kumar, S.; Ericson, L. M.; Hauge, R. H.; Smalley, R. E. Crystallization and orientation studies in polypropylene/single wall carbon nanotube composite. *Polymer* **2003**, *44*, 2373−2377.
(42) Chen, E.-C.; Wu, T.-M. Isothermal crystallization kinetics and thermal behavior of poly (ε-caprolactone)/multi-walled carbon nanotube composites. *Polym. Degrad. Stab.* **2007**, *92*, 1009−1015.
(43) Cassu, S. N.; Felisberti, M. I. Poly (vinyl alcohol) and poly (vinyl pyrrolidone) blends: Miscibility, microheterogeneity and free volume change. *Polymer* **1997**, *38*, 3907−3911.
(44) Feng, H.; Feng, Z.; Shen, L. A high resolution solid-state nmr and dsc study of miscibility and crystallization behaviour of poly (vinyl alcohol) poly (n-vinyl-2-pyrrolidone) blends. *Polymer* **1993**, *34*, 2516−2519.
(45) Zhang, X.; Takegoshi, K.; Hikichi, K. High-resolution solid-state 13 c nuclear magnetic resonance study on poly (vinyl alcohol)/poly (vinylpyrrolidone) blends. *Polymer* **1992**, *33*, 712−717.
(46) Ping, Z.-H.; Nguyen, Q. T.; Néel, J. Investigations of poly (vinyl alcohol)/poly (n-vinyl-2-pyrrolidone) blends, 1. Compatibility. *Makromol. Chem.* **1989**, *190*, 437−448.
(47) Kanagaraj, S.; Varanda, F. R.; Zhil'tsova, T. V.; Oliveira, M. S. A.; Simões, J. A. O. Mechanical properties of high density polyethylene/carbon nanotube composites. *Compos. Sci. Technol.* **2007**, *67*, 3071−3077.
(48) Kim, S. W.; Choi, H. M. Enhancement of thermal, mechanical, and barrier properties of ethylene vinyl alcohol copolymer by incorporation of graphene nanosheets effect of functionalization of graphene oxide. *High Perform. Polym.* **2015**, *27*, 694−704.
(49) Goswami, J.; Davis, V. A. Viscoelasticity of single-walled carbon nanotubes in unsaturated polyester resin: Effects of purity and chirality distribution. *Macromolecules* **2015**, *48*, 8641−8650.
(50) Jansen, R.; Wallis, P. Manufacturing, characterization and use of single walled carbon nanotubes. *Mater. Matters* **2009**, *4*, 23−27.
(51) Nepal, D.; Balasubramanian, S.; Simonian, A. L.; Davis, V. A. Strong antimicrobial coatings: Single-walled carbon nanotubes armored with biopolymers. *Nano Lett.* **2008**, *8*, 1896−1901.
(52) Kayatin, M. J. Chemical functionalization of single-walled carbon nanotubes for compatibilization with unsaturated polyester resin. Dissertation, Auburn University, 2012.

NOTE ADDED AFTER ISSUE PUBLICATION

An incorrect Supporting Information file was included with the version of this paper published April 27, 2021. The revised version was published on the Web on April 30, 2021.

https://doi.org/10.1021/acsomega.0c06174
ACS Omega 2021, 6, 10618−10628